Optical Coherence Tomography Angiography of Perilimbal Vasculature in Port-Wine Stain and Sturge-Weber Syndrome Patients

ZhanLin Zhao,[1,2] Li Xu,[1,2] XuMing Ding,[1,2] Yue Wu,[1,2] Xiangyang Zhu,[3] Yao Fu,[1,2] and WenYi Guo[1,2]

[1]Department of Ophthalmology, Ninth People's Hospital, Shanghai JiaoTong University School of Medicine, Shanghai, China
[2]Shanghai Key Laboratory of Orbital Diseases and Ocular Oncology, Shanghai, China
[3]Institute of Image Communication and Network Engineering, Shanghai Jiao Tong University, Shanghai, China

Correspondence: WenYi Guo, Department of Ophthalmology, Ninth People's Hospital, Shanghai JiaoTong University School of Medicine, Shanghai, China; wyguo@163.com.

ZZ and LX contributed equally to the work.

Received: October 24, 2019
Accepted: February 11, 2020
Published: April 28, 2020

Citation: Zhao Z, Xu L, Ding X, et al. Optical coherence tomography angiography of perilimbal vasculature in port-wine stain and Sturge-Weber syndrome patients. *Invest Ophthalmol Vis Sci.* 2020;61(4):43. https://doi.org/10.1167/iovs.61.4.43

Purpose. To evaluate episcleral vasculature in corneal limbus with optical coherence tomography angiography (OCTA) in normal controls, port-wine stain (PWS) patients, and Sturge-Weber syndrome (SWS) patients.

Methods. Unilateral eyes from 18 normal controls (25.41 ± 4.00 years), 16 PWS patients (21.35 ± 11.05 years), and 8 SWS patients with ipsilateral late-onset glaucoma (22.13 ± 7.82 years). Each subject underwent slit-lamp examination, applanation tonometry, and OCTA. All OCTA scans were performed using an OCTA system operating at a wavelength of 1050-nm in four quadrants (superior, inferior, nasal, and temporal). The scans were delineated into conjunctival and episcleral layers using IMAGEnet6 for analysis.

Results. Slit-lamp and OCTA images demonstrated dense dilated episcleral vessels in PWS and SWS patients, particularly in the SWS group. The mean limbal involvements of episcleral vascular anomalies under slit lamp were respectively 0.00 ± 0.00, 5.44 ± 2.92, and 8.88 ± 2.70 clock hours in the control, PWS, and SWS groups ($F = 58.46$, $P < 0.01$). Quantitative analysis of OCTA scans showed that the episcleral vessel density in controls, PWS, and SWS groups were 25.03% ± 1.47%, 28.28% ± 1.96%, and 33.59% ± 3.00%, respectively ($F = 18.17$, $P < 0.01$). We also observed higher episcleral vessel diameter index in the SWS and PWS groups in comparison with the controls, particularly in the SWS group ($P < 0.01$). The vessel measurements, including density and diameter, were significantly correlated with the increased IOP and cup-to-disc (C/D) in SWS patients ($P < 0.01$).

Conclusions. To our knowledge, this is the first demonstration of OCTA in PWS and SWS patients and represents direct pathoanatomic evidence for episcleral alterations in SWS patients. The episcleral vessel measurements correlated with the increased IOP and C/D in SWS patients, indicating the episcleral vascular hypertrophy may be a risk factor for glaucoma in adult SWS patients.

Keywords: OCT angiography, glaucoma anterior segment, Sturge-Weber syndrome, episcleral vasculature

Optical coherence tomography (OCT) uses low-coherence interferometry to visualize the in vivo imaging of ocular structures, and has shown rapid improvements and gained widespread usage since its introduction in 1991.[1] The interferometry generates axial depth scans (A-scans) based on the reflectivity profile of specific spatial dimensions and location of structures. An OCT cross-sectional B-scan is then acquired by laterally combining sequential A-scans.[2] More recently in 2014,[3] the first commercial optical coherence tomography angiography (OCTA) was introduced to delineate blood vessels by comparing phase speckle contrast, changes in intensity, or a variation of the full OCT signal between consecutive B-scans.[4,5]

Currently, OCTA plays a major role in various retinal vascular diseases of posterior segment,[6] such as the detection of macular or peripheral retinal nonperfusion in diabetic retinopathy and retinal venous occlusion,[7,8] and the diagnosis of choroidal neovascularization in patients with age-related macular degeneration.[9] Studies also explored its application in detection of the optic disc sector perfusion in glaucoma patients.[10,11] Although current commercial OCTA systems are not specifically designed for the anterior segment, several studies have recognized its future potential in providing rapid, noncontact evaluation of the cornea and anterior segment; corneal neovascularization,[12] conjunctival vasculature in normal eyes,[13] episcleral vasculature in dural carotid-cavernous sinus fistula,[14] malignant iris melanomas, and benign iris lesions[15] have been successfully observed

using OCTA. However, the use of OCTA in assessments of the anterior segment has not been fully explored.

Sturge-Weber syndrome (SWS), also known as encephalotrigeminal angiomatosis, is a systemic hamartomatosis (phakomatosis). It manifests as a triad of facial vascular malformation or nevus flammeus (also called facial port-wine stain [PWS]) in the ophthalmic division of the trigeminal nerve, ipsilateral occipital leptomeningeal angioma, and ocular complications.[16,17] Its incidence is reported to be between 1:50000 and 1:20000, regardless of sex.[18] Glaucoma is the main ophthalmic complication reported in SWS, with an incidence ranging from 30% to 60%.[19,20] The mechanisms underlying the ipsilateral glaucoma in SWS patients are still unclear. An increase in episcleral venous pressure (EVP) due to arteriovenous shunts and premature aging of the trabeculae in juvenile- and adult-onset patients,[21–23] and congenital malformation of the anterior chamber angle in children,[17,24] constitute the main hypotheses to explain the pathogenesis of glaucoma in SWS. Facial hemangiomas involving the entire V1 or bilateral V1 to V3 distribution region of the trigeminal nerve are thought to be a risk factor for ocular complications in SWS.[25,26] In addition, Phelps[22] believed that glaucoma is more pronounced with larger episcleral hemangiomas. Thus assessments of episcleral vascular hypertrophy in PWS/SWS patients may contribute to better prediction of the risk of glaucoma in SWS/PWS patients, and improve our understanding of the pathogenesis of its increased IOP.

The aims of this pilot study were to provide direct pathoanatomic evidence of the altered hemodynamics in PWS and SWS patients by using the novel OCTA technique, and to characterize and quantify the episcleral vascular anomalies in SWS patients with ipsilateral juvenile-onset glaucoma.

Methods

Participants of this cross-sectional observational pilot study were recruited at the Department of Ophthalmology in Shanghai Ninth People's Hospital (Shanghai, China) from June 2018 to October 2018. This study followed the tenets of the Declaration of Helsinki and was in accordance with the Health Insurance Portability and Accountability Act of 1996. The study protocol was approved by the investigational review board of Shanghai Ninth People's Hospital, Shanghai Jiaotong University School of Medicine, Shanghai, China (approval number: SH9H-2018-T24-1). Clinical trial registration was not required owing to the observational nature of the study. All enrolled subjects were informed about the aim of study, and informed consent was obtained from each patient or their guardians. Participants for the normal control group were recruited from volunteers.

Forty-two eyes of 42 participants were included in total: 18 normal controls (6 male, 12 female; mean age, 25.41 ± 4.00 years; age range, 23.10–37.01 years), 16 PWS patients (7 male, 9 female; mean age, 21.35 ± 11.05 years; age range, 11.99–50.59 years), and 8 SWS patients with ipsilateral glaucoma associated with nonacquired systemic disease or syndrome (1 male, 7 female; mean age, 22.13 ± 7.82 years; age range, 10.19–33.89 years). A detailed fundus examination was carried out in all participants, and their medical data, including basic information related to age and sex, were recorded. All patients had a minimum port-wine mark of trigeminal nerve V1 or V1 and V2 distribution. A diagnosis of PWS was made by the Department of Plastic and Reconstructive Surgery, Shanghai Ninth People's Hospital. The diagnosis of SWS is based on the diagnosis of PWS and ocular manifestations and/or cerebral complications.[27] All SWS patients enrolled in this study were diagnosed with an ipsilateral glaucoma associated with nonacquired systemic disease or syndrome using the following criteria: includes conditions predominantly of systemic disease present at birth that might be associated with ocular signs; and meets glaucoma definition.[28] The exclusion criteria were as follows: presence of ocular diseases, including dry eye, keratitis, chronic conjunctivitis, blepharoconjunctivitis, and pterygium; history of topical medication; history of contact lens wear; history of Sjögren syndrome, Stevens-Johnson syndrome, diabetes, or severe thyroid eye disease; and previous ocular trauma or ocular surgery.

Slit-Lamp Biomicroscopy

Each subject was asked to fix their eyes on four directions (upward, downward, outward, and inward), and color images of the superior, inferior, nasal, and temporal quadrants of the conjunctiva were acquired using a slit-lamp mounted digital camera system (SL-D Digital Slit-Lamp; Topcon, Tokyo, Japan). An x25 magnification image was obtained using a 45° angled beam of white light projected through a diffusion filter.

IOP Measurement

One drop of topical anesthetic (Benoxil 0.4%, Santen Pharmaceutical Co., Ltd, Osaka, Japan) was instilled into the inferior conjunctival cul-de-sac, and sodium fluorescein strips (Jingming, Tianjin, China) were used before the examination. IOP was then obtained using a Goldmann applanation tonometer, as described previously.[29]

OCTA Scanning

All OCTA scans were performed by an experienced physician (ZZ) using the swept-source DRI OCT unit (Triton; Topcon). This apparatus uses a wavelength-sweeping laser with a center wavelength of 1050 nm up to a depth of 2.6 mm. Participants were asked to open their eyes as wide as possible and follow a green indicator light in four directions (upward, downward, outward, and inward), fixing eyes each time for about 10 seconds. In case of failure or strong artifacts on images, an eye speculum (Kangning, Jiangsu, China) was used. The "OCT Macular Angiography" function was chosen to obtain 4.5- × 4.5-mm scans of superior, inferior, temporal, and nasal perilimbal areas, in which 100,000 A-scans were acquired per second with an optical axial resolution of 8 µm and lateral resolution of 20 µm. The appropriate focus was achieved by using a forehead shield and adjusting the diopter compensation lens selector to (+) without any anterior segment lens. Meanwhile, the eye auto-tracking function was turned off, as the default system was designed for the retina and choroid.

Image Analysis

All OCTA scans were processed automatically to reduce motion artifacts, such as transverse saccadic and residual axial motion, by the internal software (IMAGEnet6, version 1.22; Topcon). Representative images were selected for analysis by considering criteria, such as best focus, good

Investigative Ophthalmology & Visual Science

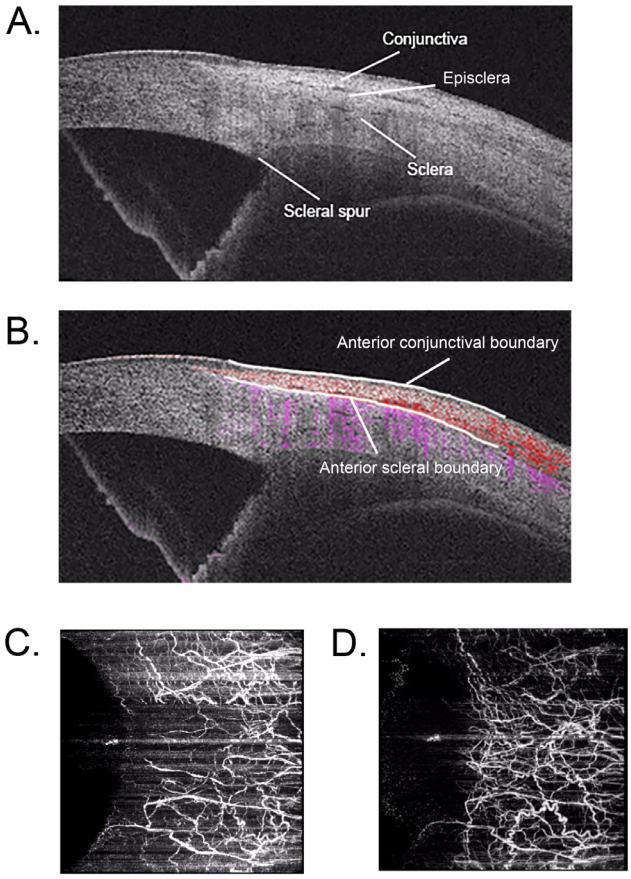

Figure 1. Delineation of OCTA scans was based on cross-sectional B-scans (**A**). Anterior conjunctival boundary and anterior scleral boundary were recognized on angio B-scans (**B**). En face conjunctival scan (**C**) was obtained from anterior conjunctival boundary to anterior scleral boundary. En face episcleral scan (**D**) was obtained from anterior scleral boundary to 100 µs under anterior scleral boundary.

contrast, and least motion artifacts with TopQ image quality above 70.

The thickness of conjunctiva varies with age, sex, and measurement location and different clinical circumstances.[30] As different structures have specific refractive index,[30] for the purpose of this study, the episcleral layer of OCTA scans was delineated based on B-scans (from anterior scleral boundary to 100 µm under anterior scleral boundary) and optimized based on en face vascular images, as shown in Figure 1.

Vessel Density and Vessel Diameter Measurements

Slit-lamp photographs: episcleral vasculature, such as engorged, dilated, or intensive blood vessels in corneal limbus under slit lamp, was noted as limbal vascular anomalies. Limbal episcleral vessel density using slit-lamp photographs were presented as the limbal involvement of episcleral vascular anomalies over 12 clock hours.

OCTA scans: a 4.5- × 4.5-mm OCTA scan (336 × 336 pixels) was performed in nasal, temporal, superior, and inferior quadrants of corneal limbus in each patient (Fig. 2A). A square of 150 × 150 pixels perpendicular to the corneal limbus, which comprises the most part of limbal vascular networks, at 3 o'clock, 6 o'clock, 9 o'clock, and 12 o'clock, was defined as the representative regions of interest (Fig. 2B). We first enhanced the OCTA image by histogram equalization and median filtering. Then a binary image was obtained from adaptive threshold binarization and morphologic process to measure vessel density (Fig. 2C). To calculate the length of the vessel, we executed skeletonization (Fig. 2D) to the vessel using Zhang-Suen Thinning Algorithm[31] with MATLAB R2010a software (The MathWorks, Inc., Natick, MA, USA). Vessel density was measured as the percentage of pixels occupied by the vessels divided by the total pixels of 150 × 150 pixels (white pixels/total pixels in the frame). The vessel diameter index was calculated as the results of vessel density divided by total vessel length.

Statistical Analysis

One-way ANOVA with the Bonferroni multiple comparisons test (GraphPad Prism version 6.00 for Mac; GraphPad, San Diego, CA, USA) was performed to compare ages, IOP, cup-to-disc (C/D) , vessel measurements data of control, PWS and SWS groups. The unit of limbal involvement of slit-lamp method was converted from clock hours to percentage (clock hours/12 clock hours) in Bland-Altman plot analysis so as to be compared with the OCTA method. The difference of episcleral vessel density between OCTA and slit-lamp methods was analyzed using Bland-Altman plots. The correlations between IOP, C/D, slit-lamp abnormal vessel quantification, and OCTA episcleral vessel measurements were analyzed using the Pearson correlation statistical test. A P value of < 0.05 was considered statistically significant. The vessel density from OCTA images was presented as means ±

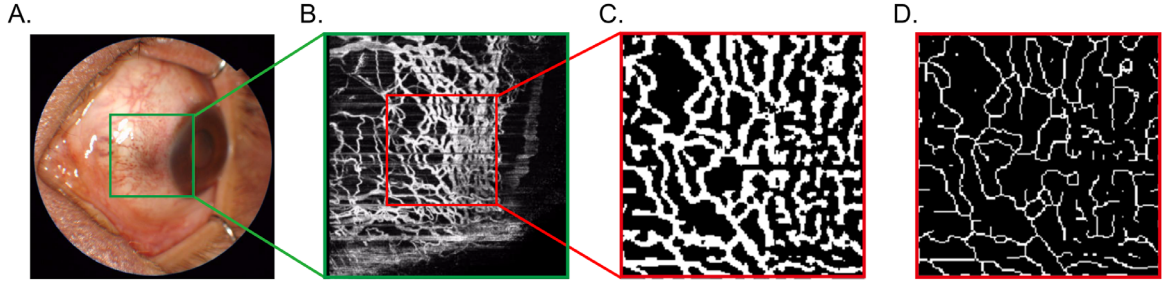

Figure 2. A 4.5 × 4.5 mm OCTA scan (336 × 336 pixels) was performed in the nasal quadrant of the corneal limbus (**A**). The region of interest is defined as 150 × 150 pixels (**B**) perpendicular to the corneal limbus at 9 o'clock. A binary image was obtained from adaptive threshold binarization and morphologic process to measure vessel density (**C**). The skeletonization was performed to obtain the total vessel length (**D**).

Investigative Ophthalmology & Visual Science

Table 1. Clinical Parameters of the Control, PWS, and SWS Groups of Study Subjects

Patient Information	Mean Age y	Number (Male /Female)	Mean Limbal Involvement Clock h	C/D Ratio	IOP mm Hg
Control	25.41 ± 4.00	18 (6/12)	0.00 ± 0.00	0.30 ± 0.05	14.72 ± 3.51
PWS	21.35 ± 11.05	16 (7/9)	5.44 ± 2.92[*,†]	0.32 ± 0.07	15.81 ± 3.82
SWS	22.13 ± 7.82	8 (1/7)	8.88 ± 2.70[‡,*,†]	0.88 ± 0.16[‡,*,†]	31.50 ± 8.70[‡,*,†]

Data are presented as mean ± StD.
[*] Compared with controls, $P < 0.01$.
[†] Compared with PWS, $P < 0.05$.
[‡] Compared with PWS, $P < 0.01$.

95% confidence interval (CI); the other data were presented as means ± StD.

Results

Demographic and Clinical Characteristics of Subjects

The demographic and clinical characteristics of the participants are summarized in Table 1. The mean C/D ratio was respectively 0.30 ± 0.05, 0.32 ± 0.07, and 0.88 ± 0.16 in the control, PWS, and SWS groups ($F = 142.2$, $P < 0.01$). The mean IOP was respectively 14.72 ± 3.51 mm Hg, 15.81 ± 3.82 mm Hg, and 31.50 ± 8.70 mm Hg in the control, PWS, and SWS groups ($F = 35.08$, $P < 0.01$). No difference was found in the C/D ratio and IOP between controls and PWS patients, whereas on the basis of the diagnostic criteria, C/D ratio and IOP were significantly higher in SWS patients than those in the controls (SWS vs. controls, $P < 0.01$) and PWS patients (SWS vs. PWS, $P < 0.01$).

Demonstration of Episcleral Vasculature

Slit-lamp photography and OCTA scans of the superior, inferior, temporal, and nasal quadrants of the limbus were performed in all participants. All OCTA scans were delineated into en face conjunctival and episcleral layers. Slit-lamp images and OCTA episcleral scans of the nasal, temporal, superior, and inferior quadrants in the control, PWS, and SWS groups are demonstrated in Figure 3. The difference of density and vessel dilation in episcleral vasculature was apparent between the control, PWS, and SWS groups (Fig. 3). Superficial episcleral plexus vessels demonstrated thin anastomoses in the controls. PWS, and particularly SWS patients, showed compact vascular network consisted of dilated episcleral vessels (Fig. 3). In addition, OCTA scans seemed to provide a more precise and clear view of episcleral anomalies compared with slit-lamp photography.

Quantification of Vessel Density

Slit-lamp photographs and OCTA scans were both analyzed for quantification of episcleral vessel density. Slit-lamp photographs showed a more important limbal involvement of abnormal episcleral vascularity in PWS and SWS patients. The mean limbal involvements of episcleral vascular anomalies were respectively 0.00 ± 0.00, 5.44 ± 2.92, and 8.88 ± 2.70 clock hours in the control, PWS, and SWS groups ($F = 58.46$, $P < 0.01$). Vascular anomalies as dilated or tortuous episcleral vessels were found both in PWS and SWS patients. The abnormal vascularity was particularly more extensive in SWS patients compared with controls and PWS patients (controls vs. SWS, $P < 0.01$; PWS vs. SWS, $P < 0.01$).

All OCTA image scans were also analyzed to assess episcleral vessel density. Quantitative analysis showed a significantly greater episcleral vessel density in SWS and PWS patients compared with normal controls (control vs. PWS, $P < 0.01$; PWS vs. SWS, $P < 0.05$; Fig. 4A). The average episcleral vessel density in the control, PWS, and SWS groups were 25.03% ± 1.47%, 28.28% ± 1.96%, and 33.59% ± 3.00%, respectively ($F = 18.17$, $P < 0.01$). The vessel densities in the superior, inferior, nasal, and temporal quadrants in the limbus of the three groups are listed in Table 2.

Correlation analysis and Bland-Altman plot analysis of the two quantification methods described earlier were performed. The extensive abnormal vasculature observed in slit-lamp photographs correlated significantly to the increased vessel density of OCTA scans ($r = 0.81$, $P < 0.01$; Fig. 4B). Bland-Altman plots showed the concordance of two quantification methods with a bias of –3.45% ± 31.70% and a 95% CI of –65.58%, 58.68% (OCTA-slit lamp; Fig. 4C), suggesting that slit-lamp method underestimated the vessel density in controls and overestimated in SWS patients than the OCTA method.

Quantification of Vessel Diameter

The mean episcleral vessel diameter index in SWS patients demonstrated a significant increase in nasal, superior, and inferior quadrants of the limbal area in comparison with normal controls (Table 3). The mean episcleral vessel diameter index was 3.52 ± 0.11, 3.68 ± 0.13, and 3.92 ± 0.24 in controls, PWS patients, and SWS patients, respectively (Fig. 5). PWS and SWS groups showed a significantly higher average vessel diameter compared with controls (PWS vs. controls, $P < 0.05$; SWS vs. controls, $P < 0.01$), particularly in the SWS group (SWS vs. PWS, $P < 0.01$).

Correlation Analysis of IOP, C/D, and Vessel Measurements

Our analysis found a positive correlation between increased episcleral vessel density and IOP ($r = 0.45$, $P < 0.01$; Fig. 6A), and between increased episcleral vessel density and C/D ratio ($r = 0.54$, $P < 0.01$; Fig. 6B). A positive correlation was also found between episcleral vessel diameter index and IOP ($r = 0.56$, $P < 0.01$; Fig. 6C), and between episcleral vessel diameter index and C/D ratio ($r = 0.65$, $P < 0.01$; Fig. 6D). Those findings demonstrated an increased IOP and C/D ratio along with a dense dilated limbal episcleral vasculature in SWS patients, suggesting the episcleral vasculature involvement in the pathogenesis of glaucoma in SWS patients.

Investigative Ophthalmology & Visual Science

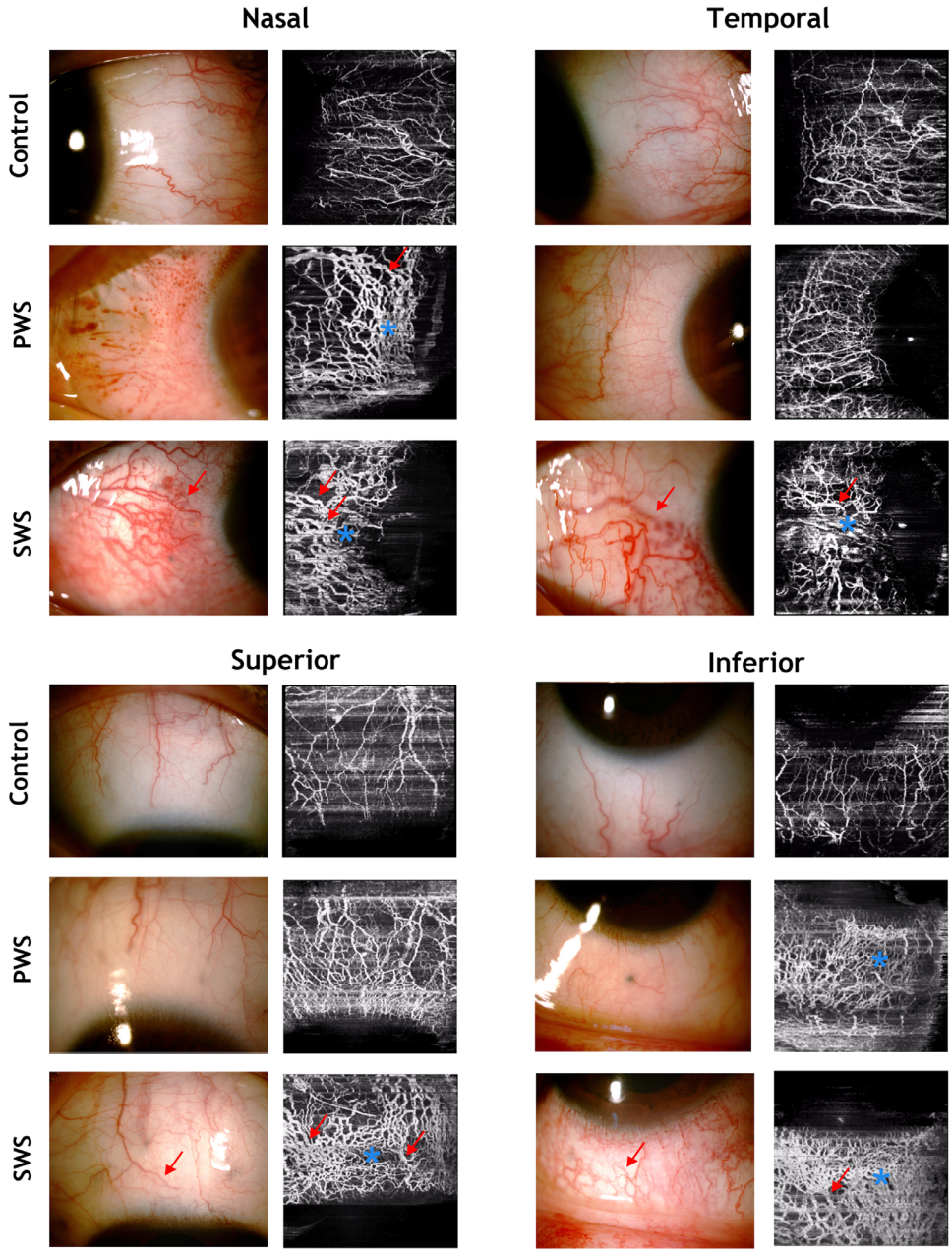

Figure 3. Demonstration of episcleral vessels of the nasal, temporal, superior, and inferior quadrants in control and PWS and SWS groups. Note the compact vascular network (*asterisks*) consisted of dilated episcleral vessels (*arrows*) in PWS and SWS patients.

Table 2. The Episcleral Vessel Density of the Superior, Inferior, Nasal, and Temporal Quadrants in the Limbus of the Three Groups

Group	Nasal Vessel Density %	Temporal Vessel Density %	Superior Vessel Density %	Inferior Vessel Density %
Control	25.06 ± 1.75	27.72 ± 2.66	21.78 ± 1.38	25.56 ± 3.16
PWS	28.44 ± 2.47	30.19 ± 2.46	27.00 ± 2.82[†]	27.50 ± 3.32
SWS	33.29 ± 4.40[†,‡]	32.75 ± 3.81	35.75 ± 3.84[†,§]	33.50 ± 4.33[*]

Data are presented as means ± 95% CI.
[*] Compared with controls, $P < 0.05$.
[†] Compared with controls, $P < 0.01$.
[‡] Compared with PWS group, $P < 0.05$.
[§] Compared with PWS group, $P < 0.01$.

Investigative Ophthalmology & Visual Science

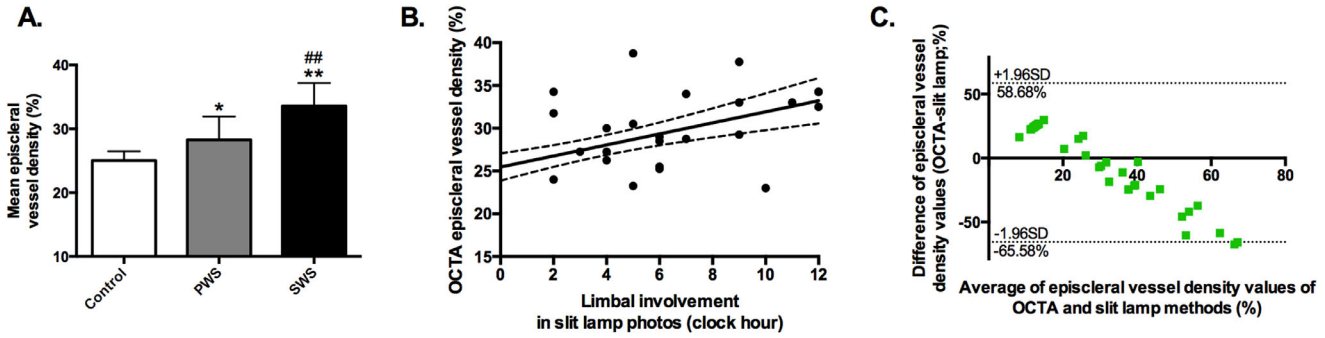

Figure 4. The mean episcleral vessel density of OCTA scans in the control, PWS, SWS groups (**A**), its correlation with limbal involvement of episcleral abnormalities using slit-lamp photographs (**B**), and Bland-Altman plots comparing OCTA and slit-lamp quantification methods (**C**). Data are presented as mean ± 95% CI. *Compared with controls, $P < 0.05$; **compared with controls, $P < 0.01$; ##compared with PWS, $P < 0.01$; $r = 0.58$, $P < 0.01$ (**B**).

Table 3. The Mean Episcleral Vessel Diameter Index of the Nasal, Temporal, Superior, and Inferior Quadrants in Controls, PWS, and SWS Patients

	Nasal Episcleral Vessel Diameter Index	Temporal Episcleral Vessel Diameter Index	Superior Episcleral Vessel Diameter Index	Inferior Episcleral Vessel Diameter Index
Control	3.49 ± 0.18	3.57 ± 0.19	3.49 ± 0.23	3.55 ± 0.22
PWS	3.63 ± 0.22	3.74 ± 0.27	3.66 ± 0.32	3.70 ± 0.24
SWS	4.02 ± 0.35*,†	3.93 ± 0.29*	3.77 ± 0.21	3.96 ± 0.42*

Data are presented as mean ± StD.
* Compared with controls, $P < 0.01$.
† Compared with PWS, $P < 0.01$.

Discussion

Episcleral venous anomalies are reported to be involved in the pathogenesis of glaucoma in SWS patients.[16–18] We applied the novel OCTA technique for visualization and analysis of the episcleral vasculature in PWS and SWS patients with juvenile-onset glaucoma.

Currently, the main assessment of anterior segment vasculature in SWS patients is restricted to slit-lamp photography and intraoperative observations. OCTA has been shown to serve as an innovative noninvasive method for evaluating blood flow and vessel density. OCTA visualize vessels of all sizes, including marginal corneal vascular arcades in the episcleral vasculature. Our findings in this study have proved the correlation and concordance between limbal involvement of episcleral abnormal vessels observed in slit-lamp photography, and the episcleral vessel density using OCTA scans (Figs. 4B, 4C). More importantly, OCTA enables respective en face delineation of conjunctival and episcleral vasculature, owing to the different optical scattering features of biologic tissues.[30] Compared with slit-lamp photography, in which underestimation of poorly visible blood vessels in the episcleral layer may occur (Fig. 2), the density quantification method described in this study is much more precise and enables furthermore the vessel diameter measurements (Figs. 4, 5). Another option for assessment of anterior segment are angiography techniques using fluorescein or indocyanine green, whereas those invasive techniques expose patients to potential adverse reactions.[32]

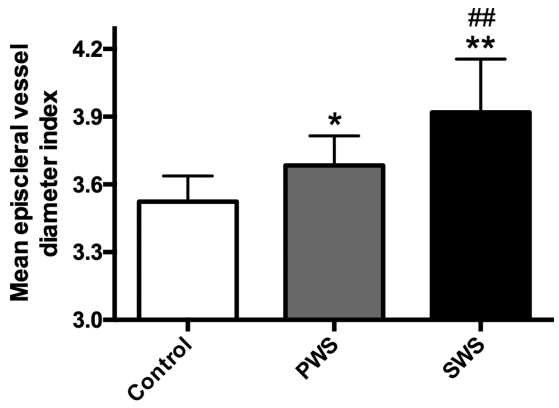

Figure 5. The mean episcleral vessel diameter index in controls, PWS, and SWS patients. Data are presented as mean ± StD. *Compared with controls, $P < 0.05$; **compared with controls, $P < 0.01$; ##compared with PWS, $P < 0.01$.

To date, different OCTA systems, such as split-spectrum amplitude-decorrelation angiography (SSADA) and spectral-domain (SD) OCTA system, have shown promising results in imaging anterior segment.[33] The SSADA and SD systems respectively run a scanning speed at 70 and 53 kHz with a wavelength at 840 and 880 nm. It should be noted that the swept-source-based OCTA in this study was less prone to motion artifacts because of its faster scanning speed (100 kHz A-scan rate),[34] and provided a better penetration through light-retaining tissues, such as the sclera or limbus, with its long wavelength (1050 nm).[15] The main limitations of this OCTA system for imaging the anterior segment are related to three points: first, good patient cooperation is required, as the scan acquisition takes approximately 10 seconds and the tracking system is not currently available for the anterior segment; second, the OCTA image size in the anterior segment was limited to 4.5 × 4.5 mm due to long

Investigative Ophthalmology & Visual Science

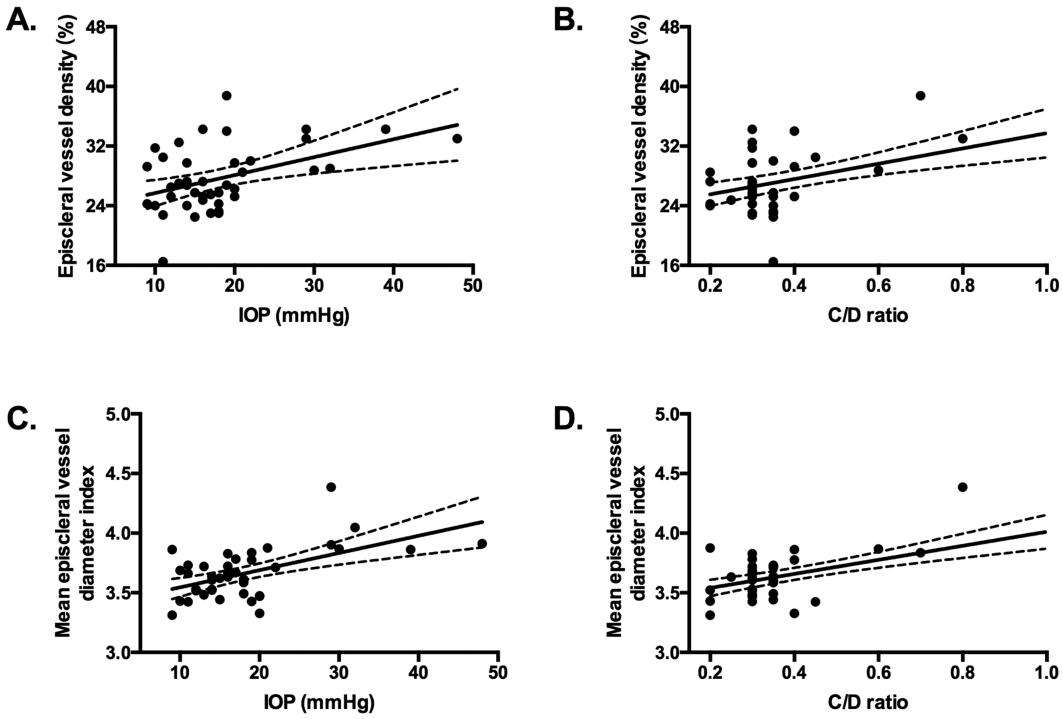

Figure 6. Increased episcleral vessel density was correlated to higher IOP (**A**; $r = 0.45$, $P < 0.01$) and C/D ratio (**B**; $r = 0.54$, $P < 0.01$). Increased episcleral vessel diameter index was correlated to higher IOP (**C**; $r = 0.56$, $P < 0.01$) and C/D ratio (**D**; $r = 0.65$, $P < 0.01$).

acquisition time and motion artifacts with 6- × 6-mm or 12- × 12-mm module so that it is not large enough to capture the entire bulbar conjunctive area; and third, the episcleral layer of OCTA scans could be slightly affected by the superficial OCTA signals, as the DRI OCT used in this study does not have a function for projection artifacts removal.

IOP is determined by evaluating the ratio of aqueous humor production to aqueous outflow. In the conventional pathway, the aqueous humor flows through the trabecular meshwork into the canal of Schlemm, then into aqueous collector channels and aqueous veins. The resistance to aqueous outflow through the trabecular meshwork is influenced by a second pressure at the level of the episcleral veins: EVP. Any obstruction of the drainage pathway may elevate EVP causing episcleral vessel dilation, which includes thyroid ophthalmopathy, episcleral or orbital vein vasculitis, cavernous sinus, and orbital vein thrombosis.[35] Contrary to the elevated EVP and episcleral vessel dilation secondary to venous obstruction, SWS is believed to lead to elevated EVP via arteriovenous anomalies itself, such as arteriovenous shunts formed within the vascular anomalies.[36–38]

The episcleral vasculature is normally characterized by the absence of capillaries, numerous arteriovenous anastomoses, and a muscle-rich venous network.[39] Akagi et al.[13] have described a Y-shaped sectoral pattern of scleral vasculature in normal corneal limbus using OCTA, which had a similar appearance to the aqueous angiography images, indicating that scleral plexus vasculature observed in OCTA scans contributes to aqueous drainage. The limbal episcleral hypertrophy from OCTA scans observed in our study reflected the arteriovenous anomalies in SWS patients. Phelps[22] proposed that the veins draining aqueous from the canal of Schlemm are a part of an episcleral vessel anomaly, or the canal of Schlemm itself may be part of the vessel anomaly in PWS and SWS patients. Our finding of linear correlation of IOP and C/D ratio with episcleral vessel measurements is in agreement with the results of previous studies,[40–42] and supports the hypothesis that progressive hypertrophy and dilatation of the episcleral veins contribute to an increase in EVP and IOP, then the ipsilateral juvenile-onset glaucoma in SWS patients.[20] In addition, the prominent episcleral vessels are related to severe surgical complications, such as choroidal effusion.[43] We propose that the limbal episcleral alteration may be a risk factor for glaucoma in adult SWS patients, and clinicians should examine carefully episcleral vasculature in terms of vessel density and vessel dilation in PWS and SWS patients.

Because of our small sample size, we did not measure the EVP values. The role of the episcleral vasculature, its specialties in regulation of IOP, and the hypotheses related to strategies for glaucoma treatment based on the mechanism of raised EVP need further investigation. Moreover, choroidal hemangioma is associated with a higher risk of glaucoma.[44] As the presence of choroidal hemangioma was not recorded for this study, we cannot comment on the relationship between choroidal hemangioma and glaucoma in SWS.

Conclusions

OCTA images demonstrate more severe dilated dense vessels in limbal episclera in SWS patients compared with PWS patients. This noninvasive technique may serve as a more precise and reliable approach alternative to conventional slit-lamp examinations for assessing episcleral vascular patterns and providing quantitative measurement of vascular anomalies. The correlation we found between IOP, C/D

Investigative Ophthalmology & Visual Science

ratio, and episcleral vessel measurements in the study indicated episcleral vascular hypertrophy in SWS patients might account for pathogenesis of glaucoma. The OCTA evaluation of episcleral vasculature may also be used for the investigation of episcleral vascular alterations in glaucoma secondary to dilated episcleral veins and relevant targeted treatment.

Acknowledgments

Supported by the National Nature Science Foundation of China grants (81970796, 81670845), the Science and Technology Commission of Shanghai (17DZ2260100), the Clinical Research Program of Medicine of Shanghai Municipal Health Commission (201940330), and the Joint Research Project of the Emerging Cutting-Edge Technology of Shanghai Shen-Kang Hospital Development Center (SHDC12018110). The authors alone are responsible for the content and writing of the article.

Disclosure: **Z. Zhao,** None; **L. Xu,** None; **X. Ding,** None; **Y. Wu,** None; **X. Zhu,** None; **Y. Fu,** None; **W. Guo,** None

References

1. Huang D, Swanson EA, Lin CP, et al. Optical coherence tomography. *Science*. 1991;254:1178–1181.
2. Ang M, Baskaran M, Werkmeister RM, et al. Anterior segment optical coherence tomography. *Prog Retin Eye Res*. 2018;66:132–156.
3. Schwartz DM, Fingler J, Kim DY, et al. Phase-variance optical coherence tomography: a technique for noninvasive angiography. *Ophthalmology*. 2014;121:180–187.
4. Chen CL, Wang RK. Optical coherence tomography based angiography [Invited]. *Biomed Optic Express*. 2017;8:1056–1082.
5. Spaide RF. Optical coherence tomography angiography. *Prog Retin Eye Res*. 2018;64:1–55.
6. Ang M, Tan ACS, Cheung CMG, et al. Optical coherence tomography angiography: a review of current and future clinical applications. *Graefes Arch Clin Exp Ophthalmol*. 2018;256:237–245.
7. Balaratnasingam C, Inoue M, Ahn S, et al. Visual acuity is correlated with the area of the foveal avascular zone in diabetic retinopathy and retinal vein occlusion. *Ophthalmology*. 2016;123:2352–2367.
8. Samara WA, Shahlaee A, Adam MK, et al. Quantification of diabetic macular ischemia using optical coherence tomography angiography and its relationship with visual acuity. *Ophthalmology*. 2017;124:235–244.
9. Sulzbacher F, Pollreisz A, Kaider A, et al. Identification and clinical role of choroidal neovascularization characteristics based on optical coherence tomography angiography. *Acta Ophthalmol*. 2017;95:414–420.
10. Jia Y, Wei E, Wang X, et al. Optical coherence tomography angiography of optic disc perfusion in glaucoma. *Ophthalmology*. 2014;121:1322–1332.
11. Liu L, Jia Y, Takusagawa HL, et al. Optical coherence tomography angiography of the peripapillary retina in glaucoma. *JAMA Ophthalmol*. 2015;133:1045–1052.
12. Ang M, Sim DA, Keane PA, et al. Optical coherence tomography angiography for anterior segment vasculature imaging. *Ophthalmology*. 2015;122:1740–1747.
13. Akagi T, Uji A, Huang AS, et al. Conjunctival and intrascleral vasculatures assessed using anterior-segment optical coherence tomography angiography in normal eyes. *Am J Ophthalmol*. 2018;196:1–9.
14. Ang M, Sng C, Milea D. Optical coherence tomography angiography in dural carotid-cavernous sinus fistula. *BMC Ophthalmol*. 2016;16:93.
15. Skalet AH, Li Y, Lu CD, et al. Optical coherence tomography angiography characteristics of iris melanocytic tumors. *Ophthalmology*. 2017;124:197–204.
16. Comi AM. Presentation, diagnosis, pathophysiology, and treatment of the neurological features of Sturge-Weber syndrome. *Neurologist*. 2011;17:179–184.
17. Sullivan TJ, Clarke MP, Morin JD. The ocular manifestations of the Sturge-Weber syndrome. *J Pediatr Ophthalmol Strabismus*. 1992;29:349–356.
18. Waelchli R, Aylett SE, Robinson K, et al. New vascular classification of port-wine stains: improving prediction of Sturge-Weber risk. *Br J Dermatol*. 2014;171:861–867.
19. Sujansky E, Conradi S. Outcome of Sturge-Weber syndrome in 52 adults. *Am J Med Genet*. 1995;57:35–45.
20. Jagtap S, Srinivas G, Harsha KJ, et al. Sturge-Weber syndrome: clinical spectrum, disease course, and outcome of 30 patients. *J Child Neurol*. 2013;28:725–731.
21. Arora KS, Quigley HA, Comi AM, et al. Increased choroidal thickness in patients with Sturge-Weber syndrome. *JAMA Ophthalmol*. 2013;131:1216–1219.
22. Phelps CD. The pathogenesis of glaucoma in Sturge-Weber syndrome. *Ophthalmology*. 1978;85:276–286.
23. Cibis GW, Tripathi RC, Tripathi BJ. Glaucoma in Sturge-Weber syndrome. *Ophthalmology*. 1984;91:1061–1071.
24. Wu Y, Yu R, Chen D, et al. Early trabeculotomy ab externo in treatment of Sturge-Weber syndrome. *Am J Ophthalmol*. 2017;182:141–146.
25. Ch'ng S, Tan ST. Facial port-wine stains: clinical stratification and risks of neuro-ocular involvement. *J Plast Reconstr Aesthet Surg*. 2008;61:889–893.
26. Piram M, Lorette G, Sirinelli D, et al. Sturge-Weber syndrome in patients with facial port-wine stain. *Pediatr Dermatol*. 2012;29:32–37.
27. Abdolrahimzadeh S, Scavella V, Felli L, et al. Ophthalmic alterations in the Sturge-Weber syndrome, Klippel-Trenaunay syndrome, and the Phakomatosi Pigmentovascularis: an independent group of conditions? *BioMed Res Int*. 2015;2015:786519.
28. Beck A, Chang TCP, Freedman S. Definition, classification, differential diagnosis. In: *Childhood Glaucoma: The 9th Consensus Report of the World Glaucoma Association*. Amsterdam, The Netherlands: Kugler Publications; 2013:5–20.
29. Francis BA, Hsieh A, Lai MY, et al. Effects of corneal thickness, corneal curvature, and intraocular pressure level on Goldmann applanation tonometry and dynamic contour tonometry. *Ophthalmology*. 2007;114:20–26.
30. Read SA, Alonso-Caneiro D, Vincent SJ, et al. Anterior eye tissue morphology: scleral and conjunctival thickness in children and young adults. *Sci Rep*. 2016;6:33796.
31. Zhang TY, Suen CY. A fast parallel algorithm for thinning digital patterns. *Commun ACM*. 1984;27;236–239.
32. Kirwan RP, Zheng Y, Tey A, et al. Quantifying changes in corneal neovascularization using fluorescein and indocyanine green angiography. *Am J Ophthalmol*. 2012;154:850–858.
33. Ang M, Devarajan K, Das S, et al. Comparison of anterior segment optical coherence tomography angiography systems for corneal vascularisation. *Br J Ophthalmol*. 2018;102:873–877.
34. Ang M, Cai Y, Tan ACS. Swept source optical coherence tomography angiography for contact lens-related corneal vascularization. *J Ophthalmol*. 2016;2016:9685297.
35. Brubaker RF. Determination of episcleral venous pressure in the eye. *Arch Ophthalmol*. 1967;77:110–114.
36. Weiss DI. Dual origin of glaucoma in encephalotrigeminal hemangiomatosis. *Trans Ophthalmol Soc UK*. 1973;93:477–493.

37. Jørgensen JS, Guthoff R. Sturge-Weber syndrome: glaucoma with elevated episcleral venous pressure. *Klin Monbl Augenheilkunde*. 1987;191:275–278
38. Shiau T, Armogan N, Yan DB, et al. The role of episcleral venous pressure in glaucoma associated with Sturge-Weber syndrome. *J AAPOS*. 2012;16:61–64.
39. Kanski JJ. *Clinical Ophthalmology*. 5th ed. Oxford: Butterworth Heinemann; 2003.
40. Mosier MA, Smythe BA. Conjunctival photocoagulation in Sturge-Weber syndrome. *Arch Ophthalmol*. 1992;110:1530–1531.
41. Sinawat S, Auvichayapat N, Auvichayapat P, et al. 12-year retrospective study of Sturge-Weber syndrome and literature review. *J Med Assoc Thai*. 2014;97:742–750.
42. Akagi T, Uji A, Okamoto Y, et al. Anterior segment optical coherence tomography angiography imaging of conjunctiva and intrasclera in treated primary open-angle glaucoma. *Am J Ophthalmol*. 2019;208:313–322.
43. Bellows AR, Chylack LT, Epstein DL, Hutchinson BT. Choroidal effusion during glaucoma surgery in patients with prominent episcleral vessels. *Arch Ophthalmol*. 1979;97:493–497.
44. Singh AD, Kaiser PK, Sears JE. Choroidal hemangioma. *Ophthalmol Clin North Am*. 2005;18:151–161.